Solid-State Electronics 200 (2023) 108547

Contents lists available at ScienceDirect

Solid State Electronics

journal homepage: www.elsevier.com/locate/sse

A proposal of quantum computing algorithm to solve Poisson equation for nanoscale devices under Neumann boundary condition ☆

Shingo Matsuo, Satofumi Souma *

Department of Electrical and Electronic Engineering, Kobe University, Kobe 657-8501, Japan

ARTICLE INFO

Keywords:
Quantum computing algorithm
HHL algorithm
Semiconductor nanowires
Poisson equation

ABSTRACT

We present an implementation study of gate-type quantum computing algorithms for the purpose of semiconductor device simulations. As one of the representative quantum algorithms we consider the use of HHL (Harrow–Hassidim–Lloyd) algorithm to solve the Poisson equation in semiconductor nanowire p–n junction under the Neumann boundary condition that the electric field is zero at the electrode boundaries. Our proposed model of the quantum gate to implement the Neumann boundary condition along with the appropriately designed non-uniform mesh grid has been found to successfully reproduce the solution obtained by conventional method.

1. Introduction

Recent progress of quantum computing technology, especially the dramatic progress of the quantum computing environment via the cloud such as in IBM Q, have been stimulating various studies on the application of intermediate-scale quantum computers, so-called NISQ (Noisy Intermediate-Scale Quantum) devices. Such research on the specific application examples of quantum computers ranges from material science simulations [1–3] to social science simulations such as finance. In any of these cases, it is important to consider how quantum computers can be used in solving equations that have been required in individual fields.

In semiconductor device simulation as well, similarly to the recent development of machine learning algorithms for device simulations [4, 5], it is important to consider the possibility of utilizing quantum computing algorithms in the long term in the future. One of such examples is the use of HHL (Harrow–Hassidim–Lloyd) algorithm [6], which is one of the applications of the quantum phase estimation algorithm, in the calculation of the potential distribution based on Poisson equation [7–10]. However, the accurate estimation of the solutions requires large number of register qubits in general [10]. Therefore it is important to consider how we can accurately calculate the Poisson's equation with fewer qubits. With such motivation we study how the HHL algorithm can be applied to solve the Poisson's equation for semiconductor nanowire structure by limited number of qubits, especially under the Neumann boundary condition that the electric field is zero at the electrode boundaries.

2. Proposed method and results

In this study we assume the semiconductor nanowire p–n junction system shown in Fig. 1, where the left and the right regions are doped into p and n type, respectively. Assuming that the electrostatic potential and the charge density is constant within the cross-sectional area S and thus depend only on the longitudinal position x, the Poisson equation is written as $\varepsilon d^2\varphi(x)/dx^2 = -\rho(x)$, where ε is the dielectric constant, $\varphi(x)$ is the electrostatic potential, and $\rho(x)$ is the charge density. By introducing the finite difference approximation, the discretized Poisson equation is derived as $-C\varphi_{i+1} + 2C\varphi_i - C\varphi_{i-1} = Q_i$, where i stands for the position grid along the x direction, $C \equiv \varepsilon S/a$ is the capacitance with a being the grid spacing, and $Q_i \equiv \rho(x_i)\,Sa$ is the charge at the ith grid.

(i) Four sites model: In order to explore the possibility to apply the HHL algorithm for the device simulation purpose, we first consider the simplest situation, where the central device region is described by four grid points spanned by $i = 1 \sim 4$, and semi-infinite leads are attached at both ends of the central region. By imposing the Neumann boundary condition that the electric field is zero at both ends of the central device region, so that $\varphi_1 = \varphi_0$ and $\varphi_5 = \varphi_4$, we obtain the matrix equation $A|\varphi\rangle = |Q\rangle$, where the potential vector $|\varphi\rangle$ and the charge vector $|Q\rangle$ are expressed by quantum bits (qubits). The capacitance matrix A is given below and is expressed by quantum gates in the HHL algorithm shown in Fig. 2 as we will explain next.

In the HHL algorithm shown in Fig. 2 the unitary operation (U) is defined by the time evolution due to the Hamiltonian matrix A, so that

☆ The review of this paper was arranged by Francisco Gamiz.

* Corresponding author.
E-mail address: ssouma@harbor.kobe-u.ac.jp (S. Souma).

https://doi.org/10.1016/j.sse.2022.108547

Available online 9 December 2022

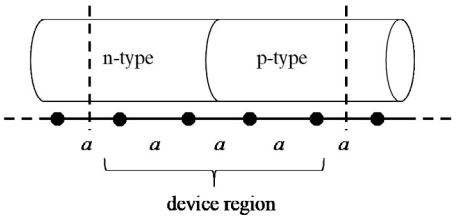

Fig. 1. Schematic illustration of the semiconductor nanowire p–n junction system, where the left and the right regions are doped into n and p types, respectively. Finite differentiated grids are also illustrated.

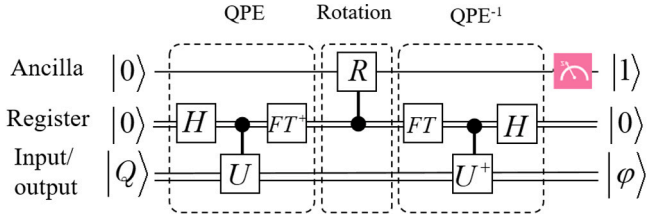

Fig. 2. Quantum gate circuit of HHL algorithm to solve matrix Poisson equation $A|\varphi\rangle = |Q\rangle$, where A is capacitance matrix and is encoded in the unitary operation U. The quantum circuit is composed of Hadamard gate (H) quantum Fourier transformation (FT), rotation (R), and unitary operation (U). If the ancilla (top most) qubit is measured to be $|1\rangle$, the solution $|\varphi\rangle$ of the linear equation is encoded in the bottom set of the qubits.

$U = e^{iAt}$. In order to implement this unitary evolution by quantum gate circuit, it is necessary to decompose the matrix A as follows.

$$A = \begin{pmatrix} \varepsilon_1 & \gamma & 0 & 0 \\ \gamma & \varepsilon_2 & \gamma & 0 \\ 0 & \gamma & \varepsilon_2 & \gamma \\ 0 & 0 & \gamma & \varepsilon_1 \end{pmatrix} = \begin{pmatrix} \varepsilon_1 & 0 & 0 & 0 \\ 0 & \varepsilon_2 & 0 & 0 \\ 0 & 0 & \varepsilon_2 & 0 \\ 0 & 0 & 0 & \varepsilon_1 \end{pmatrix} + \begin{pmatrix} 0 & \gamma & 0 & 0 \\ \gamma & 0 & 0 & 0 \\ 0 & 0 & 0 & \gamma \\ 0 & 0 & \gamma & 0 \end{pmatrix} + \begin{pmatrix} 0 & 0 & 0 & 0 \\ 0 & 0 & \gamma & 0 \\ 0 & \gamma & 0 & 0 \\ 0 & 0 & 0 & 0 \end{pmatrix}$$

$$= A_0 + A_1 + A_2, \tag{1}$$

where $\varepsilon_1 = 1$, $\varepsilon_1 = 2$, and $\gamma = -1$ in units of C. Here we note that A_0 and A_1 are operators within a single qubit, while A_2 is essentially the operator connecting two qubits (inter qubit operator). The corresponding unitary evolution operator is then calculated by applying the Trotter expansion as $U = e^{iAt} = e^{i(A_0+A_1+A_2)t} \simeq \left(e^{iA_0t/n}e^{iA_1t/n}e^{iA_2t/n}\right)^n$, where larger value of n gives more accurate results. This unitary evolution operator can be implemented by the quantum gate circuit in Fig. 3. Here we note that since the matrix A_0 is not the multiplication of the identity matrix due to the Neumann boundary condition, we propose to use the quantum gate model depicted in the $e^{iA_0t/n}$ part in Fig. 3. As for the quantum gate circuits for the quantum Fourier transformation (FT in Fig. 2) and the controlled rotation (R in Fig. 2) we employ the standard gate configurations [7].

Here it should be noted that the ith eigenvalue λ_i of the matrix A are 0, $2-\sqrt{2}$, 2, and $2+\sqrt{2}$, respectively, where the difference between adjacent eigenvalues $\Delta\lambda \equiv \lambda_{i+1} - \lambda_i$ is $\sqrt{2}$ except for the lowest one (we note that $\lambda_0 = 0$ is not required to obtain the solution $|\varphi\rangle$). We can then take the advantage of this fact if the diagonal elements of the matrix A are equally shifted by the constant $\lambda_{\rm shift} \equiv \lambda_1 - \Delta\lambda = 2 - 2\sqrt{2}$, because then the 2nd, 3rd, and 4th eigenvalues $\lambda'_i = \lambda_i - \lambda_{\rm shift}$ are given by $\lambda'_i = i\Delta\lambda = \sqrt{2}i$ and are exactly described by two-digit decimal binary numbers 0.01, 0.10, and 0.11, respectively, where 0.01 corresponds to the decimal expression 0.25 and is scaled to $\lambda'_i = i\Delta\lambda$ by the factor $\Delta\lambda/0.25$. The pre-subtracted value $\lambda_{\rm shift}$ can be re-incorporated at the controlled rotation part R to obtain the correct solution $|\varphi\rangle$. We implemented the above scheme using the quantum programming language Qiskit, and obtained the solution $|\varphi\rangle$ very close to that obtained by the conventional method as shown in Fig. 4 (see caption for detailed parameters). We note that since all of four eigenvalues in this case are exactly described by two-digit decimal binary numbers as mentioned above in principle, the number of register qubits required is also sufficient with two.

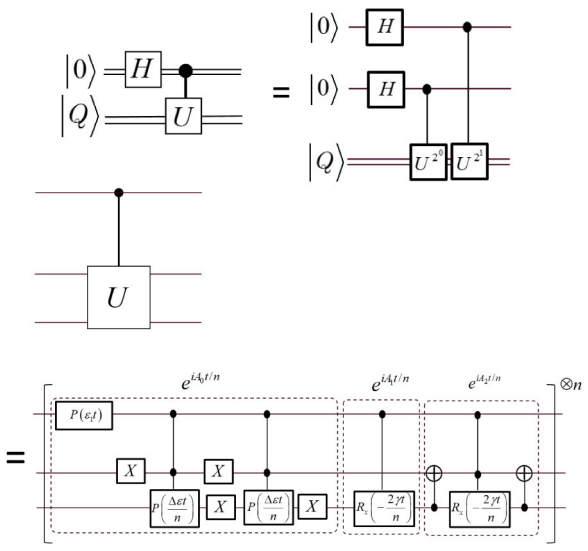

Fig. 3. Detail of the quantum circuit corresponding to the controlled unitary U part in Fig. 1. P abd R_x are the phase and x rotation gates, respectively.

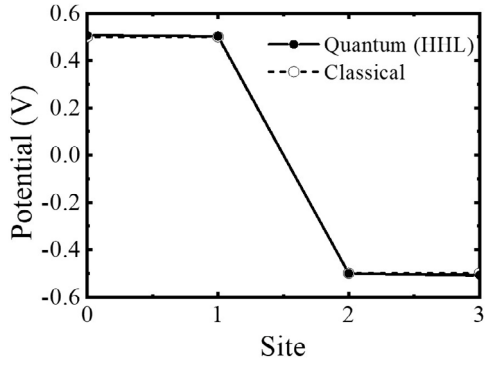

Fig. 4. Comparison of electrostatic potentials obtained by HHL and classical (exact solution in this case) methods. Here we assume that the charges of $+0.26e$ and $-0.26e$ at the 2nd and the 3rd sites, respectively. Our parameter values correspond to the case that the charge density is $\rho = 10^{26}e$ m^{-3}, grid spacing is $a = 2.6$ nm, cross-sectional area is $S = 1$ nm^2, and the material is Si. The value of n in Trotter expansion has been chosen as 16, and the time constant is $t = 2\pi \times 0.25/\sqrt{2}$.

(ii) Eight sites model: We next consider the 8 sites case, where the central device region is described by eight grid points spanned by $i = 1 \sim 8$, and semi-infinite leads with zero net charge are attached at both ends of the central region. If we simply extend the 4 sites model to the eight site model, however, the eigenvalues of the 8×8 matrix A in the linear equation $A|\varphi\rangle = |Q\rangle$ are not equally separated unlike the 4 sites case, and we cannot take the above mentioned advantage in this case. Therefore, we consider to introduce the non-uniform mesh grids in the stage of finite-difference approximation of Poisson's equation, and we adjust the grid spacing so that the adjacent eigenvalues of the 8×8 matrix A are as equally separated as possible. In the top panel of Fig. 5 we show the schematic illustration of the non-uniform 8-sites model, where the grid spacings (adjusted so that the adjacent eigenvalues

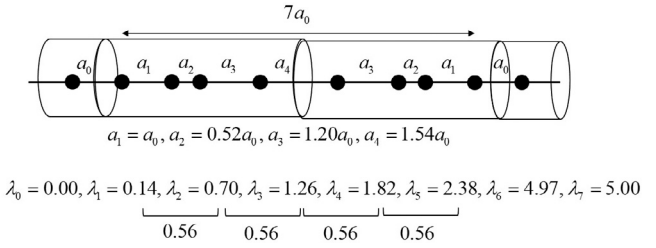

Fig. 5. (Top) Schematic illustration of the non-uniform 8-sites model, where the grid spacings are adjusted so that the adjacent eigenvalues of the 8 × 8 matrix A are as equally separated as possible. (Bottom) The calculated eigenvalues of the 8 × 8 matrix A based on the non-uniform 8-sites model. We can see that the lowest 6 eigenvalues are equally separated.

are as equally separated as possible) are listed. In the bottom panel of this figure the calculated eigenvalues of the 8 × 8 matrix A are shown, where we can see that the lower 5 eigenvalues (apart from the lowest one equal to zero) are equally separated by $\Delta\lambda = 0.56$. Then the equal shift of the diagonal elements of A by $\lambda_{\rm shift} \equiv \lambda_1 - \Delta\lambda$ gives $\lambda_i' = \lambda_i - \lambda_{\rm shift} = i\Delta\lambda$ up to $i = 5$.

In the same way as in the 4-sites model, the unitary operation $U = e^{iAt}$ is calculated as $U \equiv e^{iAt} = e^{i(A_0+A_1+A_2+A_3)t} \simeq \left(e^{iA_0t/n}e^{iA_1t/n}e^{iA_2t/n}e^{iA_3t/n}\right)^n$, with n being the Trotter number. In Fig. 6 we show the actual expressions for the matrices A_i ($i = 0, 1, 2, 3$) and the quantum gate circuits corresponding to e^{iA_it} ($i = 0, 1, 2, 3$), where $\varepsilon_{i=1} = -\gamma_1$ and $\varepsilon_{i=2,3,4} = -\left(\gamma_{i-1} + \gamma_i\right)$ with $\gamma_i = -C_0(a_i/a_0)$ and $C_0 \equiv \varepsilon S/a_0$.

We next consider the input charge vector $|Q\rangle$. In order to discuss how the spatial localization of the charge distribution (under the condition of anti-symmetricity for simplicity) influence the accuracy of the results obtained by the HHL algorithm for 8 sites model, we assume that the input charge vector $|Q\rangle$ is given by the following parametrized form

$$\begin{aligned}|Q\rangle = \Big[&\cos\theta\cos(\theta+\delta)|000\rangle + \cos\theta\sin(\theta+\delta)|001\rangle \\ &+ \sin\theta\cos(\theta+\delta)|010\rangle + \sin\theta\sin(\theta+\delta)|011\rangle \\ &- \sin\theta\sin(\theta+\delta)|100\rangle - \sin\theta\cos(\theta+\delta)|101\rangle \\ &- \cos\theta\sin(\theta+\delta)|110\rangle - \cos\theta\cos(\theta+\delta)|111\rangle \Big] / \sqrt{2}, \end{aligned} \tag{2}$$

where the phases θ and δ are adjustable parameters related to the spatial localization of the charge distribution. The phase θ (scaled as $\theta = \pi/x_\theta$ below) determines the overall charge localization [e.g., $x_\theta = 2$ ($\theta = \pi/2$) gives most localized charges near the interface of pn junction], while the phase δ (fixed as -0.05π in this study) is introduced to realize monotonically varying charge profile over sites within each of n and p regions. The input charge vector $|Q\rangle$ in Eq. (2) can be constructed by the quantum gate circuit shown in Fig. 7, which is placed at the left most part of the bottom set of qubits in Fig. 2.

Table 1
The coefficient β_i ($i = 1, 3, 5, 7$) for three different values of x_θ. We note that $\beta_i = 0$ for $i = 0, 2, 4, 6$ due to the antisymmetric charge distributions.

	β_1	β_3	β_5	β_7
$x_\theta = 3$	−0.814	0.465	−0.348	−0.017
$x_\theta = 2.5$	−0.618	0.590	−0.518	0.044
$x_\theta = 2$	−0.270	0.562	−0.777	0.087

In Fig. 8(a) and (b) we show the input charge vector $|Q\rangle$ given by Eq. (2) for various values of x_θ, and the corresponding solutions $|\varphi\rangle$, respectively. In (b) the results obtained by the quantum algorithm and the classical (conventional) algorithm are compared. As seen in Fig. 8(b), we obtained good agreement between the quantum and classical solutions except for the most localized charge distribution realized by $x_\theta = 2$. The reason behind the larger error for more localized case can be understood by analyzing the coefficient β_i in the expansion $|Q\rangle = \sum_{i=0}^{N-1}\beta_i|a_i\rangle$, where $|a_i\rangle$ is the ith eigenvector of A and $N = 2^n$ with $n = 3$ in the 8-sites model. As shown in the Table 1, we have larger value of β_7 for more localized $|Q\rangle$, meaning that in the solution $|\varphi\rangle = A^{-1}|Q\rangle = \sum_{i=1}^{N-1}\left(\beta_i/\lambda_i\right)|a_i\rangle$ the highest order $i = 7$th term contributes non-negligibly to $|\varphi\rangle$. Here we recall that the eigenvalue λ_i in the denominator can be estimated accurately only for $\lambda_{i\le 5}$ by the quantum circuit with three register qubits, where the equal separations of adjacent eigenvalues play the essential role. Therefore the non-negligible value of β_7 and the estimation error of λ_7 is the origin of the error in the quantum solution of $|\varphi\rangle$. For less localized $|Q\rangle$, on the other hand, the value of β_7 is negligibly small (e.g., for $x_\theta = 3$) and thus the estimation error of λ_7 (independent of $|Q\rangle$) does not cause significant error in the quantum solution of $|\varphi\rangle$, suggesting that for charge distributions varying moderately over sites the proposed non-uniform mesh scheme is beneficial in obtaining accurate solutions by the HHL algorithm with fewer register qubits in general.

3. Conclusion

We have presented an implementation study of HHL algorithm to solve the Poisson equation in semiconductor nanowire p–n junction

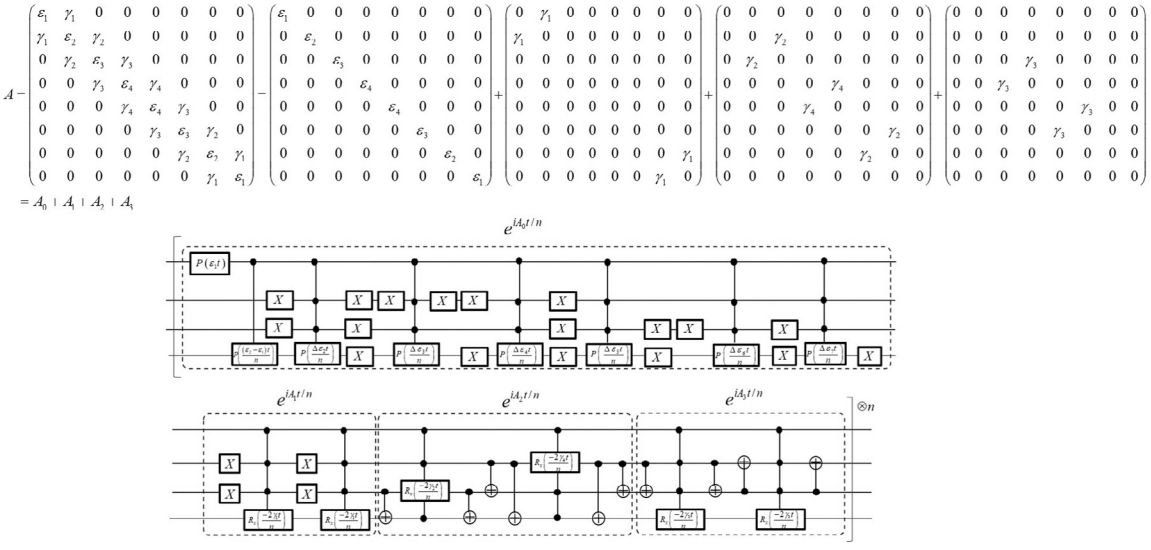

Fig. 6. (Top) The decomposition of the capacitance matrix A. (Bottom) Detail of the quantum gate circuit for the operations e^{iA_it} ($i = 0, 1, 2, 3$).

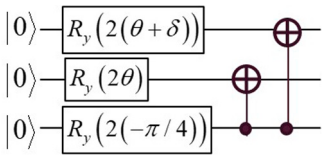

Fig. 7. Quantum gate circuit to construct the input charge vector $|Q\rangle$ in Eq. (2). The phase θ (scaled as $\theta = \pi/x_\theta$) is treated as adjustable parameters, while the phase $\delta = -0.05\pi$ is fixed value (see the text).

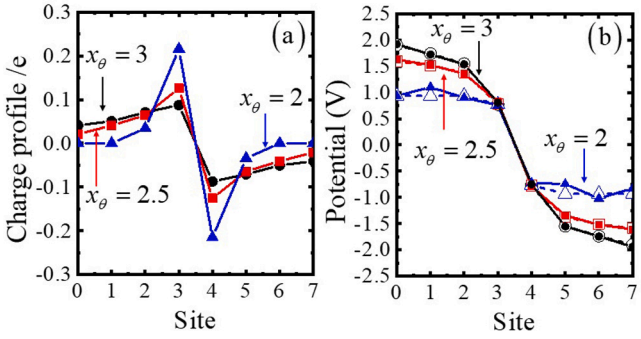

Fig. 8. (a) Input charge distributions for non-uniform 8-sites model given by Eq. (2) for various values of x_θ. We assumed that the summation of charges in each of p and n regions are equal to ± 0.25e same as the four site model. (b) Corresponding solutions $|\varphi\rangle$. In (b) the solid lines and closed symbols are used for the quantum (HHL) results, while the dashed lines and the open symbols are used for the classical (conventional) results.

under the Neumann boundary condition that the electric field is zero at the electrode boundaries. Our proposed model of the quantum gate circuit to implement the Neumann boundary condition has been found to successfully reproduce the solution obtained by conventional method for the four sites model, where the equal separation of the adjacent eigenvalues of the capacitance matrix A plays the important role. This basic idea has been extended to eight sites model by appropriately designing the non-uniform grid which allows the matrix A to have eigenvalues as equally separated as possible, and we obtained good agreement between the quantum (HHL) and classical results except for very localized charge distribution cases. These results suggest that the proposed non-uniform mesh scheme is beneficial for $N = 2^n$ sites model in general in obtaining accurate solutions by the HHL algorithm with fewer register qubits if the charge distributions varies moderately over sites.

Declaration of competing interest

The authors declare that they have no known competing financial interests or personal relationships that could have appeared to influence the work reported in this paper.

Data availability

Data will be made available on request.

Acknowledgment

This work was partially supported by JSPS, Japan KAKENHI Grant No. 22K04244.

References

[1] Ma H, Govoni M, Galli G. Npj Comput Mater 2020;6:85.
[2] Cerasoli FT, Sherbert K, Slawínska J, Nardelli MB. Phys Chem Chem Phys 2020;22:21816.
[3] Shokri S, Rafibakhsh S, Pooshgan R, Faeghi R. Eur Phys J Plus 2021;136:762.
[4] Souma S, Ogawa M. IEICE Electr Express 2020;17:20190739.
[5] Souma S, Ogawa M and. Proc. of International Conference on Simulation of Semiconductor Processes and Devices (SISPAD2021), 2021;56.
[6] Harrow AW, Hassidim A, Lloyd S. Phys Rev Lett 2009;103:150502.
[7] Wang S, Wang Z, Li W, Fan L, Wei Z, Gu Y. Quantum Inf Process 2020;19:170.
[8] Morrell H, Wong HY. Proc. of 2021 International Conference on Simulation of Semiconductor Processes and Devices (SISPAD2021), 2021;69.
[9] Lee Y, Joo J, Lee S. Sci Rep 2019;9:4778.
[10] Yalovetzky R, Minssen P, Herman D, Pistoia M. 2021, arXiv:2110.15958.